International Journal of Engineering

Journal Homepage: www.ije.ir

The Effect of Transition Metals Incorporation on the Structural and Magnetic Properties of Magnesium Oxide Nanoparticles

H. H. Hanish*, S. J. Edrees, M. M. Shukur

Department of Ceramic & Building Materials, College of Materials Engineering, University of Babylon, Hilla, Iraq

P A P E R I N F O

Paper history:
Received 16 February 2020
Received in revised form 01 March 2020
Accepted 23 March 2020

Keywords:
Diluted Magnetic Semiconductors
Magnesium Oxide
Nanomaterials
Structural Properties
Transition Metals

A B S T R A C T

Pure and doped magnesium oxide nanoparticles were successfully synthesized employing a sol-gel process. The synthesized nanoparticles were characterized by thermal differential analysis, X-ray powder diffraction, transmission electron microscopy, scanning electron microscope, energy-dispersive X-ray spectroscopy, and vibrating sample magnetometer. X-ray diffraction patterns confirmed the crystallization of MgO structure and correspondingly ratified that the transition metal atoms were incorporated into the MgO host lattice. The crystallite size decreases as the concentration of dopants were augmented. TEM images showed that the particles of pristine magnesium oxide were embedded in the sheet matrix of the graphene-like layer with a size of 22.06 nm. The EDS spectra revealed the presence of carbon in pure MgO nanoparticles, while nickel and chromium were distributed in the host lattice. Based on VSM measurements, room temperature ferromagnetism in pristine MgO-NPs could be ascribed to the presence of either Mg vacancy or carbon atoms. Furthermore, paramagnetic ordering had been observed upon doping. Overall, the prepared MgO-NPs may be found as a potential application in spintronics devices.

***doi**: 10.5829/ije.2020.33.04a.16*

1. INTRODUCTION

Recently, the concept of nanotechnology and its nanomaterials is a thriving specialty of research in a variety of fields. This field of science has the potential to breakthrough many applications such as electric and electronic devices, catalysts, optical, magnetic, and biomedical devices [1–3]. On the account of their excellent physicochemical features, high surface area to volume ratio, and distinctive nanosize structure, metal oxides nanomaterials such as TiO_2, ZnO, CuO, and MgO is being increasingly applied as an alternative agent in different applications [4, 5]. In the last decades, many studies on the preparation of metal oxides nanocrystals with large surface area and high reactivity have been offered [6]. At present, several types of metal oxides nanoparticles play very important role in numerous areas of physics, chemistry, and materials science. The numbers of metals can form a large miscellany of metal oxides. They involve the structural geometries with an electronic structure that can reveal semiconductor, metallic or insulator character [7]. In practical applications, metal oxides nanoparticles are utilized in the production of microelectronic circuits, optoelectronics, fuel cells, sensors, and piezoelectric devices [8]. MgO is considered as one of the most important among the metal oxides nanoparticles for several reasons such as nontoxicity, and relatively easy to obtain.

Magnesium oxide (MgO) has drawn wide research interest [9]. MgO nanoparticles have exhibited excessive potential as an adsorbent for toxic chemical agents [10]. It possesses unique magnetic, electronic, optical, thermal, chemical, and mechanical properties because of its excellent chemical and physical properties [11]. It will be interesting to know that bulk magnesium oxide is non-magnetic [12]. However, the nanoparticle size of magnesium oxide and other nonmagnetic oxides such as ZnO and HfO_2 show the new route of magnetism [13, 14]. Magnetic ordering demonstrated via these metals

*Corresponding Author Email: *haneenha432@gmail.com* (H. H. Hanish)

Please cite this article as: H. H. Hanish, S. J. Edrees, M. M. Shukur, The Effect of Transition Metals Incorporation on the Structural and Magnetic Properties of Magnesium Oxide Nanoparticles, International Journal of Engineering (IJE), IJE TRANSACTIONS A: Basics Vol. 33, No. 4, (April 2020) 647-656

oxides is acknowledged as d^0 ferromagnetism, as they either have filled or empty *d*-/*f* orbitals. This magnetism is supposed to take place as a result of polarization brought by *p*-orbitals, where magnetic polarization arises because of anion and/or cation vacancies [15].

Many methods have been adopted to synthesis MgO-NPs such as sol-gel [16], co-precipitation [3], and hydrothermal method [17]. The sol-gel method is an appropriate method to produce pristine and doped MgO [18]. This technique is known as a method for the formation of inorganic oxides with gel structures, which are converted to solid glass at low temperatures and can be well-defined from a thermodynamic perspective as a relatively stable solid phase formation at a certain temperature, liquid [19].

The sol-gel route has a number of benefits. Due to the handy decontamination of liquids, it is conceivable to harvest materials with high quality [20]. Materials with exceptionally good chemical homogeneity can also be produced, which are highly desirable, especially in the case of complex oxides, because the mixing of components takes place at the molecular level during chemical reactions [16]. Low condensation temperatures are another good feature. The existence of real disadvantages must not be forgotten. Initial starting materials (e.g., metal alkoxides) are somewhat expensive. Difficulties in the usual drying phase during which cracks and significant shrinkage are common problems mentioned earlier [21].

Generally, any impurities of transition metals incorporated in the host of MgO nanocrystals either as a dopant or as a solid solution may cause defects in the form of vacancies, interstitials, and antisites, which are considered the enhanced source of magnetism, electronic, optical, and thermal properties of bare MgO-NPs. The main objective of this work is to unveil the influence of nickel and chromium transition metals incorporation on the crystal structure, magnetic, and morphological properties of the prepared MgO-NPs. To bring a better understanding of the work to the readers, we organize this report as follows: Experimental method, including chemicals used, methodology and essential parameters are given in Section 2. The results and appropriate discussion are offered in Section 3, which is divided according to subsections including Thermal analysis (Subsection 3.1), Structural analysis (Subsection 3.2), Morphological analysis Subsection 3.3, and Magnetic analysis (Subsection 3.4). Finally, Section 4 summarizes the results of this work.

2. EXPERINMENTAL METHOD

2. 1. Chemicals Used Magnesium nitrate hexahydrate [$Mg(NO_3)_2{\cdot}6H_2O$] (BDH Chemicals Ltd, England, > 99% purity), nickel nitrate hexahydrate [$Ni(NO_3)_2{\cdot}6H_2O$] (Fisher Certified, > 99% purity), $Cr(NO_3)_3.9H_2O$ (CDH, India, >99%), citric acid [$C_6H_8O_7.H_2O$] (CDH, India, >99%) and high quality doubled distilled water were used to prepare pristine and doped MgO by sol-gel method. All reagents were used without any further purifications.

2. 2. Samples Preparation The pristine and doped MgO samples nanoparticles were prepared by the sol-gel method [22]. For the preparation of pristine MgO-NPs, 6.0897 g of $Mg(NO_3)_2.6H_2O$ and 5.253 g of citric acid [$C_6H_8O_7.H_2O$] were dissolved in 50 ml distilled water in two beakers separately. They were stirring for 60 min using a magnetic stirrer (FALC instrument-F91). Then, the citric acid solution was added to $Mg(NO_3)_2.6H_2O$ solution drop by drop. The mixture was kept stirring with a rotation speed of 800 rpm at 80℃ until a wet gel formed after 3 hours. The temperature and pH values of the aqueous solution were controlled using a portable multi-parameter meter (BANTE instrument-900P). Then, the white precipitate was aged overnight, washed, and centrifuged (High speed refrigerated centrifuge-GL-12) with a rotation speed of 3000 rpm for 10 min several times to remove the by-products. The magnesium hydroxide gel was dried at 130 ℃ for 3 hours. The dried powder has been calcined at 500 ℃ for 2 hours with 5 ℃/min as a heating rate using a furnace device (PIF 160/15- Made in Turkey). For the synthesis of doped and co-doped samples, 0.5 M of $Mg(NO_3)_2.6H_2O$ and various amount of transition metal nitrates, $Ni(NO_3)_2.6H_2O$ and $Cr(NO_3)_3.9H_2O$, were dissolved in 50 ml distilled water. Citric acid [$C_6H_8O_7.H_2O$] has been added to the solution drop by drop. After 3 hours, a gel was formed at a temperature of 80 ℃. The gel was dried at 130 ℃ for 4 hours and then heat-treated at 500℃ for 2 hours. Figure 1 shows the flowchart of the experimental methodology.

Differential thermal analysis (DTA) curve was recorded by Shimadzu (DTA-50) at a heating rate of 10 ˚C/min. The X-ray diffraction patterns were obtained in the range of 30˚–90° using Shimadzu-6000 diffractometer with Cu-Kα radiation (λ = 1.5406 Å) and Ni filter. The emission current of 30 mA, accelerating voltage of 40 kV, step size of 0.02° and a slow scan speed of 2 s/step were used. The experimental diffraction patterns were investigated using x'pert highscore plus (v 3.0e) software. Crystalline phases were identified by the ICDD reference database. Crystallite size and crystal defects were evaluated based on Scherrer and Williamson-Hall plot. Furthermore, the whole powder pattern fitting technique (WPPF) was also performed to evaluate the structural parameters of pure and doped samples. The morphology and the chemical compositions of the prepared samples have been revealed using scanning electron microscopy coupled with energy dispersive – X - ray spectroscopy (TESCAN MIRA3-SAMx EDX) and transmission electron microscopy (Philips CM 100). The magnetic properties have been

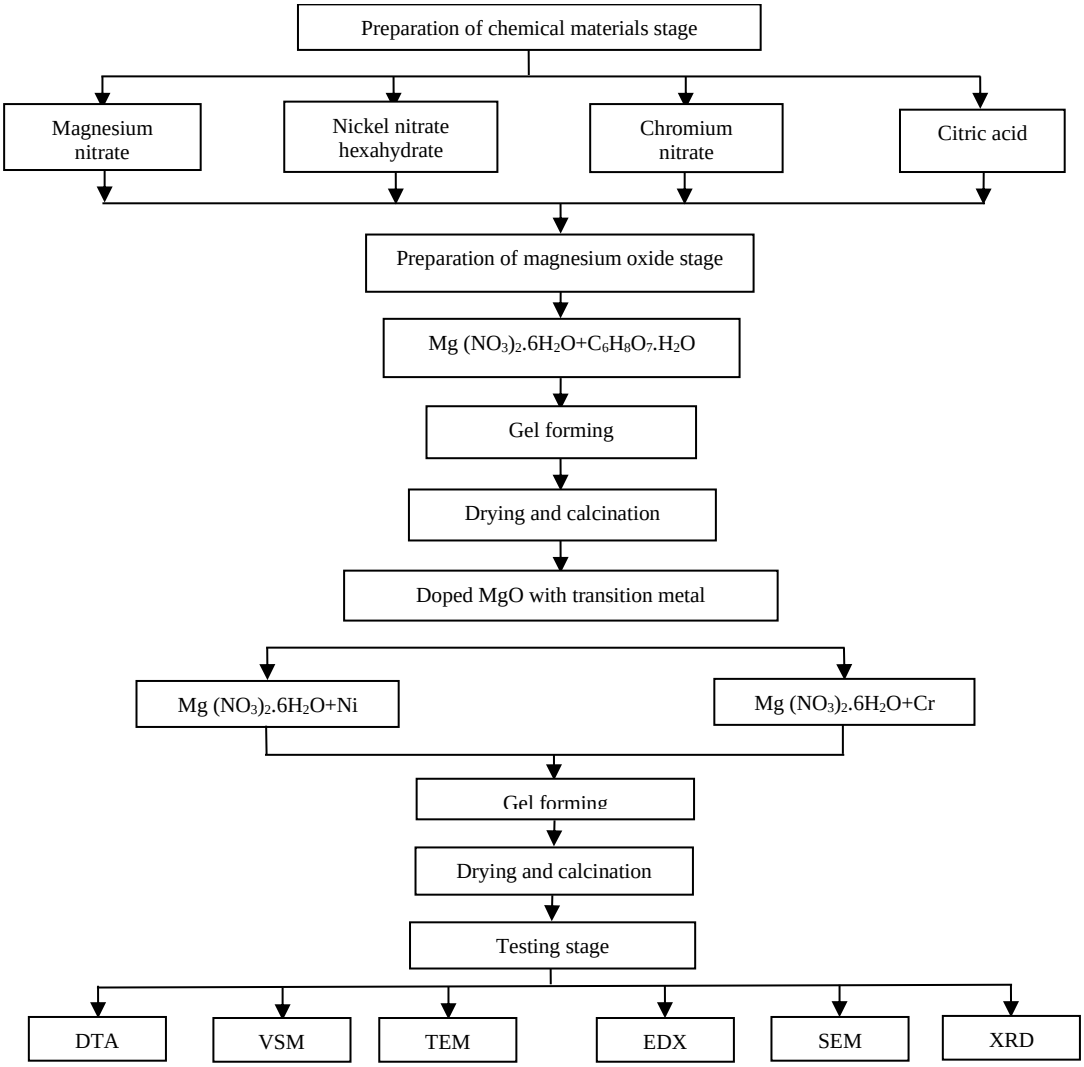

Figure 1. Flow chart of the experimental work

measured using a vibrating sample magnetometer (Cryogenic VSM).

3. RESULTS AND DISCUSSION

3. 1. Thermal Analysis The differential thermal analysis (DTA) curve of the prepared magnesium hydroxide [$Mg(OH)_2$] is illustrated in Figure 2. It is found that the thermal decomposition of magnesium hydroxide undergoes three thermal events. The first one associated with the removal of hygroscopic molecules of water, which are absorbed on the surface of $Mg(OH)_2$ particles. The adsorbing water molecules appear as a small endothermic started at 83°C. The second thermal event occurs at 314°C which represents a loss of hydroxyl ions from the structure of $Mg(OH)_2$ and converted into a distorted MgO structure. This event shows a major endothermic peak. Finally, an exothermic peak was found at 620°C and attributed to the begging order of MgO particles in a cubic structure. This observation is in good agreement with previous experimental reports [3, 23].

3. 2. Structural Analysis XRD analysis offers information about the structural characteristics of the materials as the width, and the intensity of the diffraction peaks depend on lattice strain, crystalline size, and other imperfections. The bare and doped MgO-NPs have been characterized by means of X-ray diffraction (XRD). The XRD patterns of the prepared samples are given in Figure 3(a). The diffraction peaks of samples are indexed as (111), (200), (220), (311), and (222), which is matched with ICDD PDF (no.075-0447). The samples exhibit the reflection corresponding to the cubic MgO phase having space group Fm-3m (#225). The results are in line with earlier reports [3, 23]. All patterns are in a single-phase, with no diffraction peaks from related oxides. Figure 3(b)

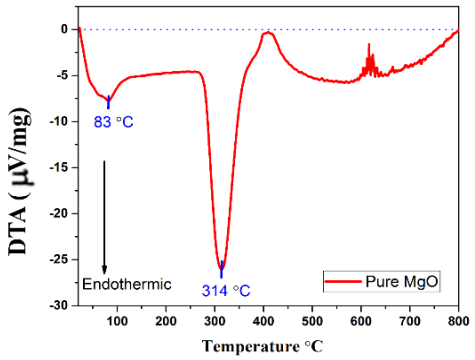

Figure 2. DTA curve of thermal decomposition of $Mg(OH)_2$ gel in the temperature range of 25-800 °C with a heating rate of 10 °C/min

exhibits the variation of XRD intensity and peak position along (200) plane with 2θ values from 41° to 45°. One can observe a heterogeneous slight shift in the peak position towards the high angles upon doping. For pristine structure, the peak is positioned at 42.69°, while for 5% Cr and 5% Ni doping, the peaks are shifted to higher 2θ positions at 42.77° and 42.79°, respectively. For the $Mg_{0.95}N_{0.04}Cr_{0.01}O$ and $Mg_{0.95}N_{0.02}Cr_{0.03}O$ samples the peaks are at 42.71° and 42.74°, respectively. It is also evident from Figure 3(b) that the intensity of the XRD peak along (200) plane gradually increased for Ni doping while it is decreased for Cr substitution. This observation may indicate that the TMs ions successfully occupy the lattice site rather than interstitial ones. This statement is in line with previous experimental report [24, 25]. The slightly shifted peak position towards higher 2θ values can be ascribed to the ionic radius difference between Ni, Cr, and Mg ions. This trend is consistent with the earlier published report [26]. The broadening of XRD reflection indicates that pristine and doped MgO-NPs are of small size. The average crystallite size (D) of the pristine and doped MgO-NPs was estimated using Scherrer's formula along (200) and (220) planes [27].

$$D = \frac{\lambda K}{\beta \cos\theta} \quad (1)$$

where D is the crystallite size, λ the X-ray wavelength of the copper anode (1.5406Å), k the shape factor (k = 0.9), [28], β the full width at half maximum (FWHM) of the diffraction peaks, and θ the Bragg diffraction angle. The broadening of the Bragg peak is a combination of both samples and instruments. To isolate these contributions, it is crucial to achieve a diffraction pattern from the line broadening of standard reference material to correct the instrumental broadening. Silicon powder was utilized to correct this influence. The instrument peak broadening of the studied MgO-NPs can be rectified according to Gaussian (strain effect), and Lorentzian (size effect) distributions [29].

For Lorentzian:

$$\beta = \beta_{obs} - \beta_{inst} \quad (2)$$

and for Gaussian:

$$\beta^2 = \beta^2_{obs} - \beta^2_{inst} \quad (3)$$

where β_{obs} is the observed peak width, and β_{inst} the instrumental broadening. When only taking into account the strain effect for the line broadening, the strain (ε) can be predicted as given below [30].

$$\varepsilon = \beta_s/4\tan\theta \quad (4)$$

Scherrer formula has some drawbacks since the impact of strain broadening is not measured. Williamson–Hall (W-H) plot delivers information about crystallite size and lattice strain. Therefore, W-H plot was adopted to estimate the lattice strain and crystallite size through the following relation [5]:

$$\beta\cos\theta = (k\lambda/D) + 4\varepsilon\sin\theta \quad (5)$$

Crystallite size and microstrain are measured from y-intercept and slope, respectively. It has been stated in the literature that a negative slope in the plot designates the presence of compressive strain, while positive slope shows the possibility of tensile strain (Figure 4). For pristine MgO-NPs, the obtained crystallite size is between 4 and 4.8 nm. This result is in good agreement with previous experimental calculations [31]. The crystallite size of the doped samples is decreased slightly as compared to the pure state. For all samples, one may perceive that the crystallite sizes measured by the W-H plot are smaller than those calculated by Scherrer expression since the latter does not uncover the influence of lattice defects on the XRD peaks broadening (Table 1). It is obvious from the scattered points in Figure 4 that the data do not fully obey the W–H formulation for different samples, where they demonstrate a non-monotonous increase of $\beta \cos\theta$ versus $4\sin\theta$. This indicates that the broadening of Bragg peaks with respect to different Bragg reflections are anisotropic and triggered by anisotropic microstrain [5]. Thus, the microstrain anisotropy observed in these nanoparticles is attributed to the occurrence of point defects.

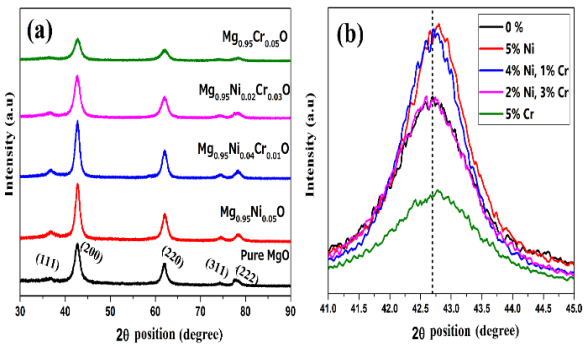

Figure 3. (a) XRD patterns of the pure and TMs doped MgO-NPs calcined at 500℃ for 2h, (b) shows slight shift in the XRD peak along (200) plane at varying doping concentrations.

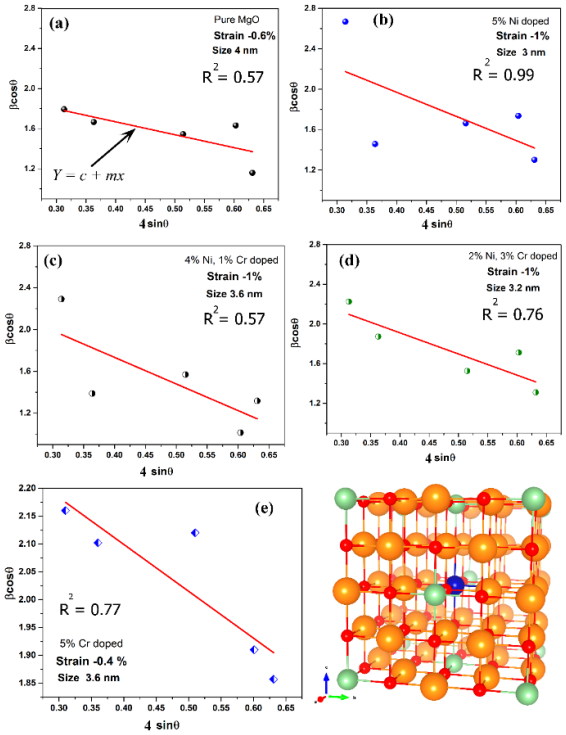

Figure 4. Williamson-Hall Plot for (a) pristine, (b) 5% Ni, (c) 4% Ni, 1% Cr, (d) 2% Ni, 3% Cr, and 5% Cr doped MgO-NPs. The last panel represents the crystal structure of the doped MgO-NPs where orange, red, green and blue represents the Mg, O, Ni, and Cr atoms.

Rietveld refinement was executed to study in detail the crystalline structure, counting both the structural (site occupancy, cell parameters, atomic position, etc) and microstructural parameters (crystallite size, microstrain, etc). The main objective of utilizing the Rietveld analysis is to reduce the difference between the calculated and observed powder diffraction pattern, see Figure 5. The minimization was performed by means of the agreement indices parameters; R_{wp} (weigh pattern factor), R_B (Bragg's angle), R_{exp} (expected error factor), and the goodness of fit (GOF). These parameters along with the occupancy of the atoms are listed in Table 2. The values of these parameters indicate that derived samples are of high quality, and refinements are effective [5]. Observed and calculated values were good matching as can be recognized from figures. Refined atomic positions indicate the presence of Mg vacancy associated with the pristine structure. Cation vacancy may induce room-temperature ferromagnetism. Furthermore, the $Mg_{0.095}Ni_{0.05}O$ and $Mg_{0.95}Ni_{0.04}Cr_{0.01}O$ samples may show the existence of an oxygen vacancy.

Lattice parameters decrease as the doping concentration increases. As presented in Figure 6, a decrease in lattice parameters relies on the ionic radius, which can be happened if the ionic radius to some extent smaller than that of the host lattice. One can perceive a slight shift of the position in the diffraction peaks representing a slight variation in lattice parameters. The values of the refined lattice parameters are in good agreement with previous experimental results [32]. The slight variation of lattice parameters with doping may indicate the existence of point defects. Dislocation density augments with impurities where it is anticipated to disturb the physicochemical properties of the

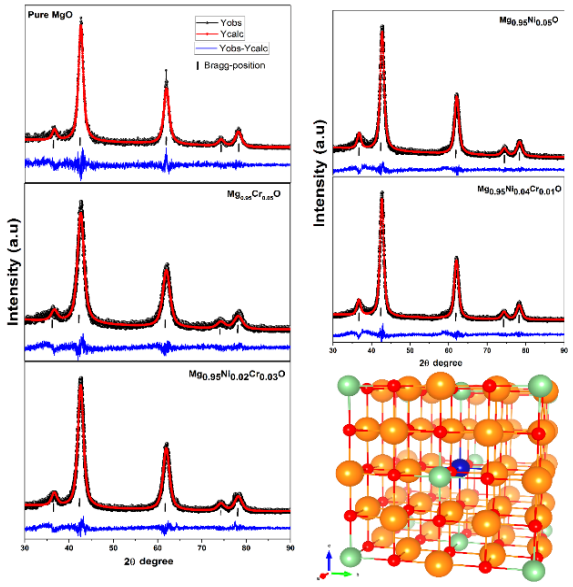

Figure 5. Rietveld refined XRD patterns of the pure and doped MgO nanoparticles. The last panel represents the crystal structure of the doped MgO-NPs where orange, red, green and blue represents the Mg, O, Ni, and Cr atoms

TABLE 1. Structural Parameters for pure and doped MgO nanoparticle from XRD measurement

Compounds	Density (g/cm^3)	W-H plot		Scherrer	Dislocation density (nm^{-1})
		Strain (%) $<\varepsilon^2>^{1/2}$ (10^{-4})	Size (nm)	Size (nm)	
Pure MgO	3.5124	-0.6	4	4.8	0.0625
$Mg_{0.95}Ni_{0.05}O$	3.7440	-1	3	5	0.111
$Mg_{0.95}Cr_{0.05}O$	3.6557	-1	3.6	3.4	0.0771
$Mg_{0.95}Ni_{0.04}Cr_{0.01}O$	3.6728	-1	3.2	5.1	0.0976
$Mg_{0.95}Ni_{0.02}Cr_{0.03}O$	3.7376	-0.4	3.6	3.9	0.0771

TABLE 2. Rietveld refinement result of pure and doped MgO-NPs calcined at 500℃

Compound	R_{exp} %`	R_B%	R_{wp} %	GOF	Site occupancy (SOF)	Lattice parameter (Å)
Pure MgO	13.5093	12.02703	16.15499	1.43003	O 1.0 Mg 0.984441	4.226
$Mg_{0.095}Ni_{0.05}O$	7.4562	7.23128	9.70809	1.69524	Mg 0.958266 Ni 0.054923 O 0.992547	4.221
$Mg_{0.095}Cr_{0.05}O$	11.4525	10.16903	13.80209	1.45239	Mg 0.9472274 Cr 0.048577 O 1.0	4.226
$Mg_{0.95}Ni_{0.04}Cr_{0.01}O$	8.2652	8.26998	11.38103	1.89604	Mg 0.955847 Ni 0.043787 Cr 0.013528 O 0.990524	4.225
$Mg_{0.95}Ni_{0.02}Cr_{0.03}O$	9.01573	8.36426	11.52438	1.63393	Mg 0.948252 Ni 0.019099 Cr 0.029068 O 1.0	4.221

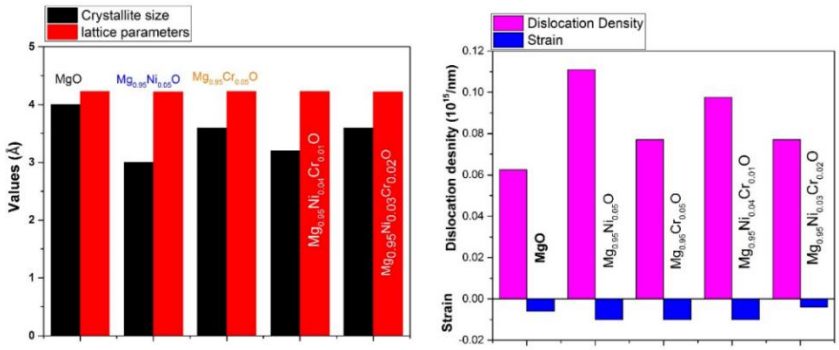

Figure 6. (a) Comparison of average lattice parameters (Å) and crystallite size (nm), (b) Comparison of average dislocation density (10^{15} / m^2) and strain% as a function of doping concentration

synthesized products. At this end, it is important to investigate dislocation density (ρ), which is defined as the length of dislocation lines per unit volume and can be estimated using the Williamson–Smallman equation, as given below [29, 33]:

$$\rho = 1/D^2 \quad (6)$$

where ρ is the dislocation density, and D the crystallite size. It can be seen that the dislocation increases, as the doping concentration increase, especially for Ni impurity density.

3. 3. Morphology Analysis Figure 7 shows the field-emission scanning electron microscope (FE-SEM) images of the pristine and doped MgO nanocrystals. Generally, the growth mechanism of nanoparticles is extremely attractive because of their large surface to volume ratio. Agglomeration process can be suppressed to control the size of nanoparticles by the introduction of organic molecules during the synthesis process [34]. The SEM images showed that the doped MgO nanoparticles have a plate-like morphology.

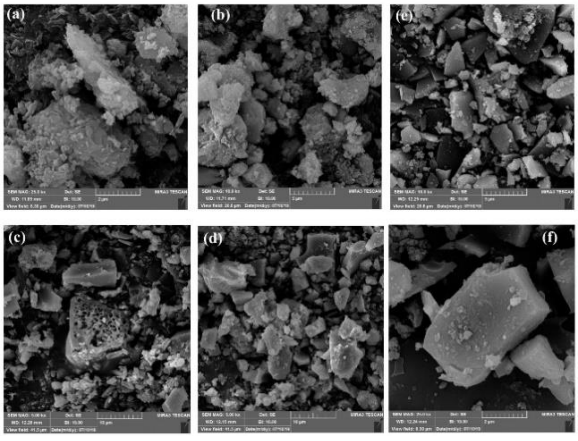

Figure 7. SEM micrographs. (a) Pure MgO, (b) $Mg_{0.95}Ni_{0.05}O$, (c) $Mg_{0.95}Cr_{0.05}O$, (d) $Mg_{0.95}Ni_{0.04}Cr_{0.01}O$, (e) $Mg_{0.95}Ni_{0.02}Cr_{0.03}O$, (f) higher magnification of $Mg_{0.95}Ni_{0.02}Cr_{0.03}O$ (e)

The elemental compositions of pure and doped MgO-NPs are determined with energy-dispersive X-ray

spectroscopy (EDS), as displayed in Figure 8. EDS is a surface-sensitive technique and it typically offers elemental composition existent up to few layers from the surface. In stoichiometric MgO, the Mg/O atomic percentage composition is 50/50 [32]. The EDS spectrum from the MgO synthesized by the aqueous method shows carbon impurities in addition to the expected magnesium and excess oxygen (Figure 8(a)). Thus, an excess amount of carbon and oxygen envisages the presence of organic citric acid in pure MgO-NPs. Furthermore, the existence of dopants in the MgO host lattice has also been confirmed, see Figure 8(b). Both nickel and chromium are detected with a minor amount of carbon compared to the bare state. This can be perceived in the TEM images.

Figure 9 shows the transmission electron microscope (TEM) images of pure MgO and TM doped MgO. TEM images have been adopted to visualize the size and shape of the nanoparticles. Since the nanoparticles are prepared without any surfactant, agglomerated ions persist in the prepared sample. This is observed clearly in the TEM image, where the particles of pristine magnesium oxide are embedded in the sheet matrix of the graphene-like layer with a size of 22.06 nm, in Figure 9(a, c). The origin of the graphene-like layer is due to the use of citric acid as a chelating agent. A similar observation has been reported by Singh et al. [34]. The TEM image of the prepared doped nanoparticles is shown in Figure 9(b). The later shows a clear decrease in particle size (12.65 nm) with better dispersion (less amount of carbon layer) compared to pristine crystal structure. This is confirmed by the EDS quantitative analysis. One may also observe that crystallite size from XRD line profiles is smaller than the particle size achieved from TEM analysis. This is related to the agglomeration of lots of small domains to form a particle [5].

3. 4. Magnetic Anslysis The magnetic properties of pure and doped MgO-NPs have studied at room temperature from magnetic-filed (*M-H*) hysteresis loops, as shown in Figure 10. For pure MgO-NPs, the hysteresis loop shows a clear ferromagnetic ordering at room temperature. Since bulk MgO is a diamagnetic insulator, the origin of this demeanor at the nanoscale can be ascribed to the existence of defects. Extensive theoretical and experimental studies show that Mg vacancy is possibly the origin of the magnetism in pristine MgO host lattice [13, 35, 36]. Nanograins of MgO are ferromagnetic, which is ascribed to the formation of cation vacancies at the surface [37]. In its bulk form, Mg and O atoms are periodically arranged conserving octahedral symmetry [15]. The periodicity may be broken in MgO nanocrystals due to the high surface area of the nanoparticles. Owing to the disorder of symmetry on the surface, Mg and O atoms are roughly bonded to the surface, and therefore easily disconnected from the surface. This may affect Mg and/or O vacancies on the surface of MgO nanoparticles. Even if we assume that MgO-NPs contain both Mg and oxygen vacancies, it is the Mg vacancy which is introducing ferromagnetic ordering. Theoretically, it is showed that Mg vacancy encourages spin polarization of 2p electrons of oxygen atoms around Mg vacancy, causing ferromagnetism in MgO host lattice [36]. Accordingly, it is the Mg vacancy that has a significant influence on the detected room temperature ferromagnetism [13]. In our study, the presence of Mg vacancy in MgO-NPs has been confirmed by Rietveld refinement, see Table 2. Other studies show that carbon atoms doped MgO crystal may induce room temperature ferromagnetism [38, 39]. Based on our quantitative EDS calculations, pristine MgO-NPs contain high inclusions of carbon atoms. Thus, carbon atoms may enhance the ferromagnetic ordering of the defected MgO-NPs. This observation may lead to more theoretical and experimental studies to unravel the cause of ferromagnetic ordering in diamagnetic MgO nanoparticles. We believe that the presence of complex defects (V_{Mg} -Carbon) is responsible for such intriguing behavior. The calculated magnetic moment of pristine MgO-NPs is 0.39 emu/g, while the coercive field (H_C) and remnant magnetization (M_r) are 55 Oe and 0.03

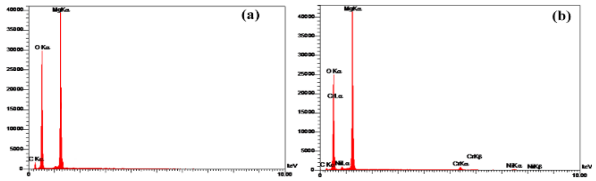

Element	Wt %	At %
C (Ka)	6.75	10.64
Mg (Ka)	50.19	39.07
O (Ka)	43.06	50.29

Element	Wt %	At %
C (Ka)	3.04	5.06
Mg (Ka)	57.56	47.38
O (Ka)	37.41	46.80
Ni (Ka)	0.34	0.12
Cr (Ka)	1.66	0.64

Figure 8. EDS spectra shows elemental composition of (a) pure MgO, (b) $Mg_{0.95}Ni_{0.02}Cr_{0.03}O$ nanoparticles

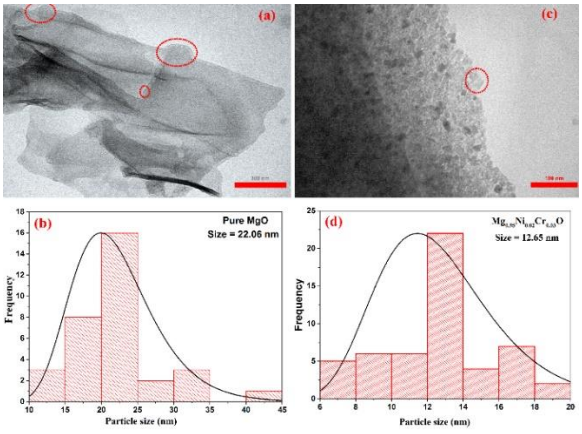

Figure 9. (a-b) TEM images and histogram particle size distribution of pure MgO, (c-d) $Mg_{0.95}Ni_{0.02}Cr_{0.03}O$ nanoparticles

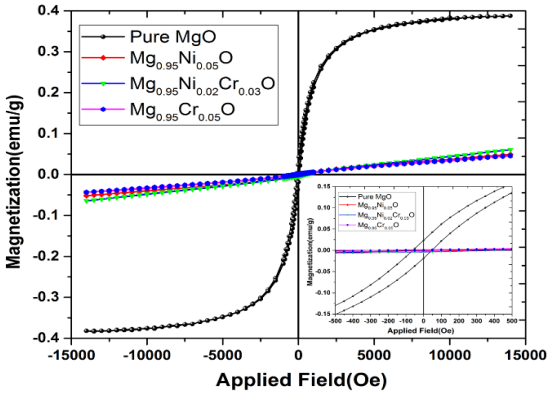

Figure 10. Room temperature magnetic field dependent magnetization (M-H) curve of pure and doped MgO-NPS

emu/g, respectively. These values are in acceptable agreement with the previous experimental results [13]. Upon doping, the hysteresis loops appear to be linear indicating the paramagnetic ordering at room temperature. The paramagnetic ordering of 5% Ni^{2+} doped MgO is in good agreement with the previous experimental report. This is consistent with the non-interacting Ni^{2+} or Cr^{3+} ions that are occupying the substitutional Mg^{2+} sites. Narayan et al. [40] suggested that the presence of the cation/anion vacancy may mediate ferromagnetic ordering in Ni-doped MgO. In our study, the presence of Mg vacancy and carbon inclusions in doped samples are less compared to that of pristine MgO structure. This observation has been long-established by Rietveld analysis and EDS measurements (Figure 8 and Table 2). The prepared MgO-NPs can be found a potential application in spintronics devices due to the presence of room temperature ferromagnetic ordering.

4. CONCLUSIONS

In the present work, pure and doped MgO-NPs have been synthesized via a facile sol-gel method. The incorporation of transition metal ions was confirmed by the X-ray diffraction technique. These nanoparticles exhibit the rocksalt phase of MgO without the presence of secondary phases. The morphologies and the elemental composition of the prepared samples were studied by TEM and FSEM coupled with the EDX technique. The TEM findings supported the XRD results indicating the nanoparticles decrease in size with increasing doping content. The hysteresis loop of the pure MgO nanoparticles shows a ferromagnetic ordering at room temperature, which can be ascribed to the presence of either Mg vacancy or carbon atoms. Furthermore, complex defects may also play a role in such an intriguing phenomenon. On the other hand, paramagnetic ordering has been observed upon doping. Thus, a very cheap and facile synthesis route is adopted to prepare ferromagnetic MgO nanoparticles that are suitable for magnetic applications.

5. ACKNOWLEDGMENT

The authors appreciate the distinguished role made by Mr. Mohammed M. Obeid who performed the experimental analysis of the prepared samples and help to discuss the results of the revised version.

6. REFERENCES

1. Karavasilis, M. and Tsakiroglou, C. D., "Synthesis of Aqueous Suspensions of Zero-Valent Iron Nanoparticles (nZVI) from Plant Extracts: Experimental Study and Numerical Modeling", ***Emerging Science Journal***, Vol. 3, No. 6, (2019), 344–360.
2. Beidokhti, M., Naeeni, S. and AbdiGhahroudi, M., "Biosorption of Nickel (II) from aqueous solutions onto Pistachio Hull waste as a low-cost biosorbent", ***Civil Engineering Journal***, Vol. 5, No. 2, (2019), 447–457.
3. Obeid, M.M., Edrees, S.J. and Shukur, M. M., "Synthesis and characterization of pure and cobalt doped magnesium oxide nanoparticles: Insight from experimental and theoretical investigation", ***Superlattices and Microstructures***, Vol. 122, (2018), 124–139.
4. Scharnberg, A.R.A., de Loreto, A.C. and Alves, A. K., "Optical and Structural Characterization of Bi2FexNbO7 Nanoparticles for Environmental Applications", ***Emerging Science Journal***, Vol. 4, No. 1, (2010), 11–17.
5. Obeid, M.M., Jappor, H.R., Al-Marzoki, K., Al-Hydary, I.A., Edrees, S.J. and Shukur, M. M., "Unraveling the effect of Gd doping on the structural, optical, and magnetic properties of ZnO based diluted magnetic semiconductor nanorods", ***RSC Advances***, Vol. 9, No. 57, (2019), 33207–33221.
6. Huang, L., Li, D.Q., Lin, Y.J., Wei, M., Evans, D.G. and Duan, X., "Controllable preparation of Nano-MgO and investigation of its bactericidal properties", ***Journal of Inorganic Biochemistry***, Vol. 99, No. 5, (2005), 986–993.
7. D'Souza, L.A.W.R.E.N.C.E. and Richards, R., "Synthesis of metal-oxide nanoparticles: liquid–solid transformations," In: Synthesis, properties, and applications of oxide nanomaterials. Hoboken, New Jersey: John Wiley & Sons, Inc., (2007), 81–117.
8. Morales, A., Lopez, T. and Gomez, R., "Crystalline structure of MgO prepared by the sol-gel technique with different hydrolysis catalysts", ***Journal of Solid State Chemistry***, Vol. 115, No. 2, (1995), 411–415.
9. Rajagopalan, S., Koper, O., Decker, S. and Klabunde, K. J., "Nanocrystalline metal oxides as destructive adsorbents for organophosphorus compounds at ambient temperatures", ***Chemistry–A European Journal***, Vol. 8, No. 11, (2002), 2602–2607.
10. Utamapanya, S., Klabunde, K.J. and Schlup, J. R., "Nanoscale metal oxide particles/clusters as chemical reagents; Synthesis and properties of ultrahigh surface area magnesium hydroxide and magnesium oxide", ***Chemistry of Materials***, Vol. 3, No. 1, (1991), 175–181.
11. Zhang, Y., Ma, M., Zhang, X., Wang, B. and Liu, R., "Synthesis, characterization, and catalytic property of nanosized MgO flakes with different shapes", ***Journal of Alloys and Compounds***, Vol. 590, (2014), 373–379.

12. Varshney, D. and Dwivedi, S., "On the synthesis, structural, optical and magnetic properties of nano-size Zn–MgO", ***Superlattices and Microstructures***, Vol. 85, (2015), 886–893.
13. Hu, J., Zhang, Z., Zhao, M., Qin, H. and Jiang, M., "Room-temperature ferromagnetism in MgO nanocrystalline powders", ***Applied Physics Letters***, Vol. 93, No. 19, (2008), 1–3.
14. Glinchuk, M.D., Eliseev, E.A., Khist, V.V. and Morozovska, A. N., "Ferromagnetism induced by magnetic vacancies as a size effect in thin films of nonmagnetic oxides", ***Thin solid films***, Vol. 534, (2013), 685–692.
15. Singh, J.P. and Chae, K. H., "d° ferromagnetism of magnesium oxidep", ***Condensed Matter***, Vol. 2, No. 36, (2017), 1–13.
16. Wahab, R., Ansari, S.G., Dar, M.A., Kim, Y.S. and Shin, H.S., "Synthesis of magnesium oxide nanoparticles by sol-gel process, In Materials Science Forum (Vol. 558), Trans Tech Publications Ltd.," (2007), , 983–986.
17. Cui, H., Wu, X., Chen, Y. and Boughton, R. I., "Synthesis and characterization of mesoporous MgO by template-free hydrothermal method", ***Materials Research Bulletin***, Vol. 50, (2014), 307–311.
18. Fu, M., Li, Y., Lu, P., Liu, J. and Dong, F., "Sol–gel preparation and enhanced photocatalytic performance of Cu-doped ZnO nanoparticles", ***Applied Surface Science***, Vol. 258, No. 4, (2011), 1587–1591.
19. Shin, D.Y. and Kim, K. N., "Electrical and optical properties of MgO films deposited on soda lime glass by a sol-gel process using magnesium acetate", ***Journal of Ceramic Processing Research***, Vol. 10, No. 4, (2009), 536–540.
20. Mbarki, R., Mnif, A. and Hamzaoui, A. H., "Structural, dielectric relaxation and electrical conductivity behavior in MgO powders synthesized by sol–gel", ***Materials Science in Semiconductor Processing***, Vol. 29, (2015), 300–306.
21. Choudhury, B. and Choudhury, A., "Microstructural, optical and magnetic properties study of nanocrystalline MgO", ***Materials Research Express***, Vol. 1, No. 2, (2014), 1–11.
22. Cai, Y., Wu, D., Zhu, X., Wang, W., Tan, F., Chen, J., Qiao, X. and Qiu, X., "Sol-gel preparation of Ag-doped MgO nanoparticles with high efficiency for bacterial inactivation", ***Ceramics International***, Vol. 43, No. 1, (2017), 1066–1072.
23. Wang, W., Qiao, X., Chen, J. and Li, H., "Facile synthesis of magnesium oxide nanoplates via chemical precipitation", ***Materials Letters***, Vol. 61, No. 14–15, (2007), 3218–3220.
24. Wang, W., Qiao, X., Chen, J. and Tan, F., "Preparation and characterization of Ti-doped MgO nanopowders by a modified coprecipitation method", ***Journal of Alloys and Compounds***, Vol. 461, No. 1–2, (2008), 542–546.
25. Islam, I., Khandy, S.A., Zaman, M.B., Gupta, D.C., Hafiz, A.K. and Siddiqui, A. M., "Effect of 3d transition metal doping (Co, Ni and Cu) on structural, optical, morphological and dielectric properties of sol–gel assisted auto-combusted Mg 0.95 Mn 0.05 O nanoparticles", ***Journal of Materials Science: Materials in Electronics***, Vol. 29, No. 5, (2018), 3952–3956.
26. Sivasankari, J., Selvakumar, S., Sivaji, K. and Sankar, S., "Structural and optical characterization of MgO: X (X= Li, Na, and K) by solution combustion technique", ***Journal of Alloys and Compounds***, Vol. 616, (2014), 51–57.
27. Hargreaves, J. S. J., "Some considerations related to the use of the Scherrer equation in powder X-ray diffraction as applied to heterogeneous catalysts", ***Catalysis, Structure & Reactivity***, Vol. 2, No. 1–4, (2016), 33–37.
28. Saravanakumar, S., Saravanan, R. and Sasikumar, S., "Effect of sintering temperature on the magnetic properties and charge density distribution of nano-NiO", ***Chemical Papers***, Vol. 68, No. 6, (2014), 788–797.
29. Hassanien, A.S., Akl, A.A. and Sáaedi, A. H., "Synthesis, crystallography, microstructure, crystal defects, and morphology of Bi x Zn 1− x O nanoparticles prepared by sol–gel technique", ***CrystEngComm***, Vol. 20, No. 12, (2018), 1716–1730.
30. Rajender, G. and Giri, P. K., "Strain induced phase formation, microstructural evolution and bandgap narrowing in strained TiO2 nanocrystals grown by ball milling", ***Journal of Alloys and Compounds***, Vol. 676, (2016), 591–600.
31. Montero, J.M., Gai, P., Wilson, K. and Lee, A. F., "Structure-sensitive biodiesel synthesis over MgO nanocrystals", ***Green Chemistry***, Vol. 11, No. 2, (2009), 265–268.
32. Dar, M.A. and Varshney, D., "Structures and properties of Mg 0.95 Mn 0.01 TM 0.04 O (TM= Co, Ni, and Cu) nanoparticles synthesized by sol–gel auto combustion technique", ***RSC Advances***, Vol. 8, No. 25, (2018), 14120–14128.
33. Williamson, G.K. and Smallman, R. E., "III. Dislocation densities in some annealed and cold-worked metals from measurements on the X-ray debye-scherrer spectrum", ***Philosophical Magazine***, Vol. 1, No. 1, (1956), 34–46.
34. Singh, J.P., Kim, S.H., Kang, H.K., Won, S.O., Lee, I.J. and Chae, K. H., "Are organic templates responsible for the optical and magnetic response of MgO nanoparticles?", ***Materials Chemistry Frontiers***, Vol. 2, No. 9, (2018), 1707–1715.
35. Martínez-Boubeta, C., Beltrán, J.I., Balcells, L., Konstantinović, Z., Valencia, S., Schmitz, D., Arbiol, J., Estrade, S., Cornil, J. and Martínez, B., "Ferromagnetism in transparent thin films of MgO", ***Physical Review B***, Vol. 82, No. 2, (2010), 1–7.
36. Gao, F., Hu, J., Yang, C., Zheng, Y., Qin, H., Sun, L., Kong, X. and Jiang, M., "First-principles study of magnetism driven by intrinsic defects in MgO", ***Solid State Communications***, Vol. 149, No. 21–22, (2009), 855–858.
37. Devaraja, P.B., Avadhani, D.N., Nagabhushana, H., Prashantha, S.C., Sharma, S.C., Nagabhushana, B.M., Nagaswarupa, H.P. and Prasad, B. D., "Luminescence properties of MgO: Fe3+ nanopowders for WLEDs under NUV excitation prepared via propellant combustion route", ***Journal of Radiation Research and Applied Sciences***, Vol. 8, No. 3, (2015), 362–373.
38. Droghetti, A. and Sanvito, S., "Electron doping and magnetic moment formation in N-and C-doped MgO", ***Applied Physics Letters***, Vol. 94, No. 25, (2009), 1–4.
39. Zhang, Y.F., Liu, H., Wu, J. and Zuo, X., "Ab Initio Study on Nitrogen or Carbon Doped Magnesium Oxide", ***IEEE Transactions on Magnetics***, Vol. 47, No. 10, (2011), 2928–2930.
40. Narayan, J., Nori, S., Pandya, D.K., Avasthi, D.K. and Smirnov, A. I., "Defect dependent ferromagnetism in MgO doped with Ni and Co", ***Applied Physics Letters***, Vol. 93, No. 8, (2008), 082507–082507.

Persian Abstract

چکیده

نانوذرات اکسید منیزیم خالص و دوپ شده با استفاده از یک فرایند سل-ژل با موفقیت تولید شدند. نانوذرات سنتزشده با تحلیل دیفرانسیل حرارتی، پراش پرتوی ایکس، میکروسکوپ الکترونی عبوری، میکروسکوپ الکترونی روبشی، طیف‌سنجی پرتوی ایکس، پراکندگی انرژی و مغناطیس‌سنج ارتعاش نمونه مشخص می‌شوند. الگوهای پراش پرتوی ایکس تبلور ساختار MgO را تأیید کرده و به همین ترتیب تأیید کرد که اتم‌های فلز انتقالی در شبکه‌ی میزبان MgO گنجانیده شده اند. اندازه‌ی بلوری با افزایش غلظت دوپانت کاهش می‌یابد. تصاویر میکروسکوپ الکترونی عبوری نشان داد که ذرات اکسید منیزیم بکر در شبکه‌ی ورق‌ای گرافن‌گونه با اندازه‌ی ۲۲/۰۶ نانومتر جا گرفته است. طیف پرتوی ایکس حضور کربن در نانوذرات MgO خالص را نشان داد، در حالی که نیکل و کرم در شبکه‌ی میزبان توزیع می‌شود. بر اساس اندازه‌گیری‌های VSM و فرومغناطیس دمای اتاق در MgO-NP های بکر را می‌توان به جای خالی منیزیم یا حضور اتم‌های کربن نسبت داد. علاوه بر این، نظم پارامغناطیسی هنگام دوپینگ مشاهده شده بود. به‌طورکلی، MgO-NP تهیه شده ممکن است به عنوان یک کاربرد بالقوه در دستگاه‌های اسپینترونیک مطرح شود.